Phase Equilibria and Multiphase Reaction Diffusion in the Cr-C and Cr-N Systems

W. Mayr, W. Lengauer, P. Ettmayer, D. Rafaja, J. Bauer, and M. Bohn

(Submitted 10 July 1998)

The phase formation in the Cr-C and Cr-N systems was investigated using reaction diffusion couples. The carbides were prepared by reaction of chromium metal with graphite powder in the range 1143 to 1413 °C in argon atmosphere; the nitride samples by reaction of the metal with N_2 (≤31 bar) in the range 1155 to 1420 °C. While the carbide samples showed the three chromium carbide phases in form of dense diffusion layers between 1100 and 1400 °C, porosity occurred at temperatures above 1400 °C. The composition of the phase bands was measured by the means of electron probe microanalysis. For the $Cr_{23}C_6$ phase, a slightly higher C composition was found than given in the literature. In Cr-N diffusion couples both the δCrN_{1-x} and βCr_2N formed phase bands at $T \geq 1150$ °C. Because decomposition processes occurred upon cooling, quenching experiments were carried out in the range 1370 to 1420 °C at 31 bar N_2 to stabilize the phases. The EPMA investigations of the homogeneity ranges yielded a large increase of the homogeneity range for δCrN_{1-x} with increasing temperature. The nonmetal diffusion coefficients in all phases of both systems were calculated from layer growth and/or from concentration profiles. In δCrN_{1-x} the N diffusivity was found to be strongly dependent on the composition. The Vickers microhardnesses of the various phases were obtained by measuring the diffusion layers.

1. Introduction

Many attempts have been made to gain information on the Cr-C and Cr-N systems because of their technical importance. A compilation of most of these studies is given by [90Ven] and by [96Neu]. Whereas crystallographic and thermodynamic data on these systems are available, no detailed investigations on the narrow homogeneity regions of the phases $Cr_{23}C_6$, Cr_7C_3, and Cr_3C_2 have been performed. Although reaction diffusion experiments were carried out by [68Fri], there are no data on the C diffusivities in chromium carbides because of the complex situation of simultaneous layer growth of all three carbide phases. In case of the Cr-N system, diffusivity data on the βCr_2N phase are available [67Sch, 81Mil], but data for δCrN_{1-x} are lacking.

In the work described in this article, the Cr-C and the Cr-N systems were investigated using diffusion couples. This technique is well suited for a simultaneous investigation of both homogeneity ranges and nonmetal diffusivities [95Len].

2. Experimental

2.1 Sample Preparation

For chromium carbide diffusion couples, Cr granules (99.8%, Heraeus, Germany) and high-purity spectral graphite powder (VSPC, Ringsdorff, Germany) were used as starting compounds. The Cr granules were arc melted in argon atmosphere to obtain buttonlike ingots. For the preparation of $Cr_{23}C_6$, Cr_7C_3, and Cr_3C_2, Cr_3C_2 powder (13.0 wt.% C, H.C.Starck, Germany) and Cr granules were used. Plane-sheet and wedge-type samples of Cr metal and of chromium carbides were packed into high-purity graphite powder in a crucible made of Mo and Zr foil and annealed from 1143 to 1413 °C in high-purity argon atmosphere in a high-temperature autoclave. The thickness of the plane-sheet samples was between 200 and 3000 μm, while the wedges were about 10 to 15 mm long and had an angle of about 15 to 20°. The temperature was measured with a Pt/Pt10%Rh thermocouple or a two-color infrared pyrometer which were calibrated against each other; the argon pressure was measured by a piezoelectric gage. About 3 to 4 min were required to heat the samples to the desired reaction temperature; subsequent cooling to ~1000 °C (at this temperature the C diffusion is rather slow) lasted about 1 min depending on the annealing temperature.

The Cr-N diffusion couples were prepared from Cr metal and high-purity N_2 in the same way as described above. The reaction temperature varied between 1155 and 1420 °C; the pressure was as much as 31 bar N_2. To perform quenching experiments, a high-temperature autoclave was equipped with a silica glass lid (Heraeus Herasil III, 40 mm diameter, 15 mm height, Germany) in which two holes were drilled into which INVAR pins (INVAR alloy, Goodfellow, GB) were glued. Inside, the pins were connected with a thin steel wire (80 μm diameter) onto which a Pt wire was mounted which in turn suspended the sample in the center of the heating zone. Outside, the pins were connected to an electrical supply line. Upon switching on the electrical current, the steel wire melted and the sample fell into liquid Sn located on the bottom of the autoclave in a silica crucible. This construction also permitted

W. Mayr, W. Lengauer, and **P. Ettmayer,** Institute for Chemical Technology of Inorganic Materials, Vienna University of Technology, Getreidemarkt 9/161, A-1060 Vienna, Austria; **D. Rafaja,** Department of Semiconductor Physics, Charles University Prague, Ke Karlovu 5, CZ-12116 Prague, Czech Republic; **J. Bauer,** Laboratoire de Chimie du Solide et Inorganique Moléculaire—CNRS-UMR 6511, Université de Rennes I, Avenue Général Leclerc, F-35042 Rennes, France; and **M. Bohn,** IFREMER, Centre de Brest, CNRS-UMR 6538, F-29280 Plouzané/Brest, France. Corresponding author, W. Lengauer, e-mail: wl@metec3.tuwien.ac.at.

a direct sight onto the sample allowing optical temperature measurement.

2.2 Metallography and Microhardness

The samples were cleaned (to eliminate carbide specimens from adhering graphite powder) in an ultrasonic bath and then embedded into a cold-setting resin. They were then cut with a diamond saw parallel to the main diffusion direction, embedded into the resin again, and ground with 40 and 20 μm diamond disks. Polishing was performed with 3 μm diamond paste and finally with an aqueous suspension of SiO_2. To improve the phase band identification in the light microscope, the samples were contrasted with lead oxide or etched with Murakami's solution at elevated temperature.

The Vickers microhardness was investigated at room temperature at a load of 9.81 N on the polished surface of the samples.

2.3 X-Ray Diffraction (XRD)

The plane samples were examined by means of XRD in Bragg-Brentano geometry with Cu Kα radiation. A graphite secondary monochromator was used. To suppress the influence of large crystallites on the diffraction pattern, a rotating sample holder was used. X-ray diffraction patterns were taken every 10 to 15 μm to investigate the phase band sequence as a function of the depth. After each scan the embedded samples were carefully ground with a 20 μm diamond disk to remove stepwise layers parallel to the surface.

2.4 Electron Probe Microanalysis (EPMA)

Microprobe analysis was performed with a Cameca Camebax SX50 microprobe in a line scan mode with a step size ranging from 3 to 10 μm. A W/Si multilayer crystal was used for the C Kα and the N Kα lines and a LIF crystal for the Cr Kα line. Further details of EPMA on diffusion couples are given elsewhere [97Len]. A 200 μm thick pure Cr sheet packed in high-purity graphite powder was annealed for 62 h at 1350 °C to prepare a Cr_3C_2 standard, which was used for the calibration routine as well as pure Cr metal. For the Cr-N system, a 200 μm Cr sheet, annealed for 263.5 h at 1229 °C and 30.7 bar N_2, was used as the δCrN_{1-x} standard. More detailed information on the peak positions, accelerating voltage, beam current, and counting time is given in Table 1.

3. Results and Discussion

3.1 Layer Formation and Morphology

Cr-C System. For temperatures up to 1374 °C, the chromium carbide diffusion couples consisted of a Cr(C) core and three dense diffusion layers of the chromium carbide phases $Cr_{23}C_6$, Cr_7C_3, and Cr_3C_2 (Fig. 1). In Fig. 1, it can be clearly seen the intermediate phase Cr_7C_3 is about twice as thick as both other layers. This result is in agreement with the work of

Table 1 Measurement conditions on the Cr-C and Cr-N systems

Element	System	Crystal	Peak position, 10^{-5} sin Θ	+Background position, 10^{-5} sin Θ	–Background position, 10^{-5} sin Θ	Background slope	Beam current (I), nA	Accelerating voltage (U), kV	Counting time (t), s
C	Cr-C	PC1	74,189	6500	6500	…	150	8	8
Cr	Cr-C	LIF	56,874	600	0	1.2	150	8	10
N	Cr-N	PC1	52,914	6500	6500	…	100	12	8
Cr	Cr-N	LIF	56,872	600	0	1.2	100	12	10

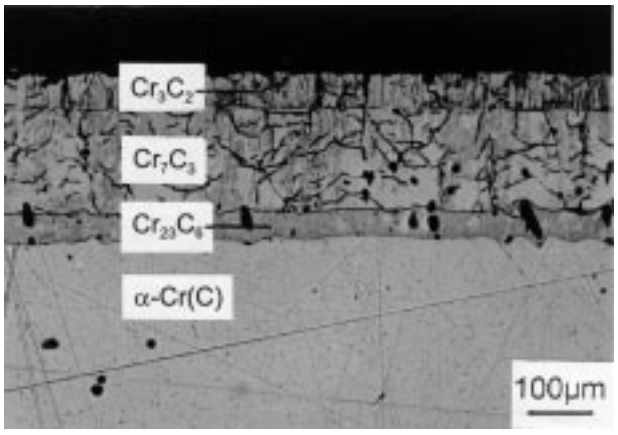

Fig. 1 Microstructure of a Cr/C diffusion couple annealed at 1262 °C for 381.0 h. The sample was etched with Murakami's solution at elevated temperature. The phase bands of Cr_3C_2, Cr_7C_3, and $Cr_{23}C_6$ are present.

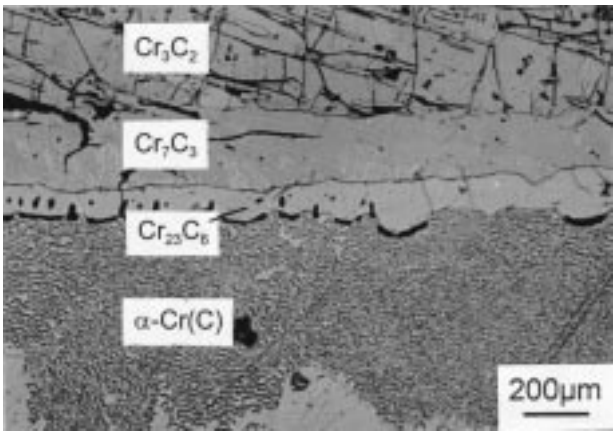

Fig. 2 Microstructure of a Cr_3C_2/Cr couple annealed at 1351 °C for 48.0 h. The phase bands of Cr_3C_2, Cr_7C_3, and $Cr_{23}C_6$ as well as the Cr(C) are present. The sample was etched with Murakami's solution at elevated temperature.

[68Fri]. This is valid for quasi-infinite sample geometry. When the $Cr_{23}C_6$ phase disappeared towards the tip of a wedge-type sample a thickness enhancement of the Cr_3C_2 phase was observed. A similar effect has been found for many other carbide and nitride phases [93Len, 96Raf, 98Wie].

At a temperature of 1413 °C, high porosity at the $Cr_{23}C_6$/Cr(C) interface occurred leading to a reduced C flux through the $Cr_{23}C_6$/Cr(C) interface. In this case, no C diffusion data could be obtained. Porosity was also observed if $Cr_{23}C_6$/C and Cr_7C_3/C couples were annealed in the range 1400 to 1500 °C. Interestingly, upon using Cr_3C_2/Cr couples, completely dense chromium carbide layers could be obtained (Fig. 2).

Cr-N System. In the Cr-N diffusion couples, the βCr_2N and δCrN_{1-x} layers were observed at $T \geq 1155$ °C (Fig. 3a). Below this temperature, a continuous CrN_{1-x} layer did not form because of its very low growth rate. At temperatures above 1200 °C, δCrN_{1-x} formed a distinct phase band that decomposed into βCr_2N and δCrN_{1-x} during cooling to room temperature. If the annealing temperature was up to 1292 °C, an extremely fine two-phase microstructure was obtained that cannot be resolved in the light microscope (Fig. 3b). At higher annealing temperatures (1420 °C) the decomposition led to a coarser two-phase microstructure, with βCr_2N at the original δCrN_{1-x} grain boundaries and small oriented βCr_2N precipitates within the δCrN_{1-x} grains (Fig. 3c). At intermediate temperatures, that

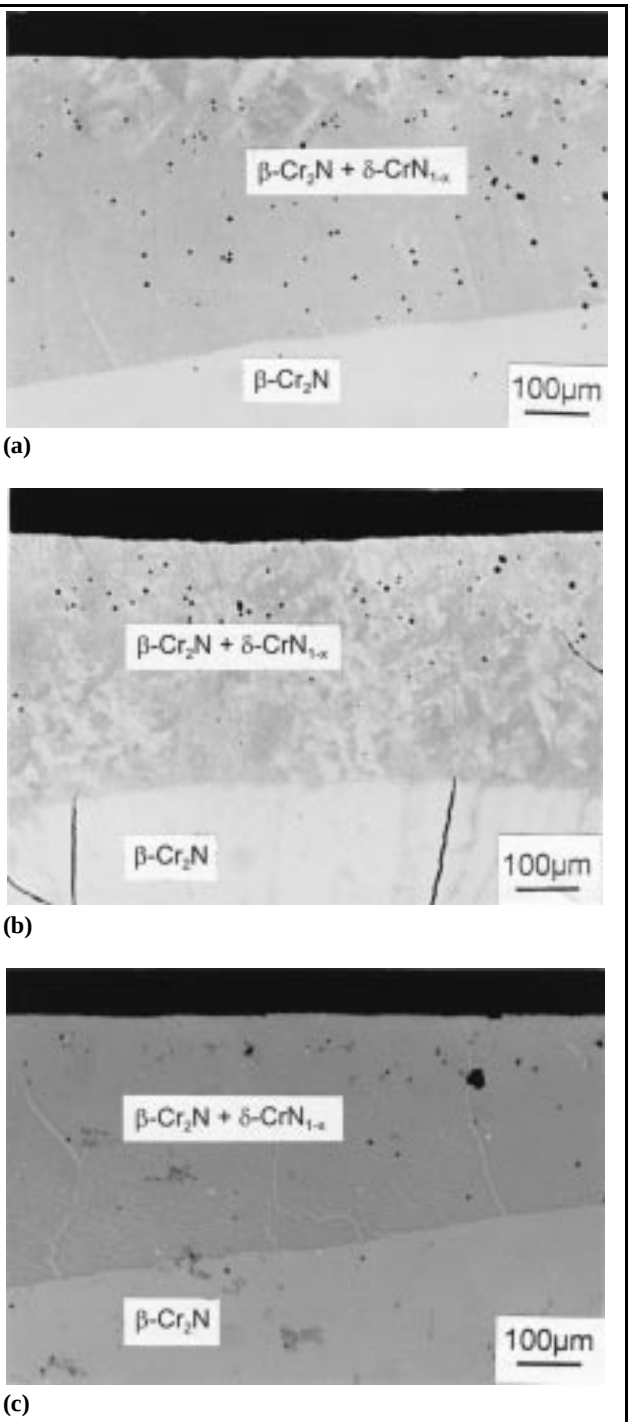

Fig. 3 Cr/N diffusion couples showing the different microstructures of the decomposition of the δCrN_{1-x} phase (etched with Murakami's solution at elevated temperature, polarized light). (a) Annealed at 1369 °C, 30.9 bar N_2 for 24.4 h, coarse and fine microstructure. (b) Annealed at 1292 °C, 31.1 bar N_2 for 50.5 h, fine microstructure. (c) Annealed at 1422 °C, 31.0 bar N_2 for 7.8 h, coarse microstructure

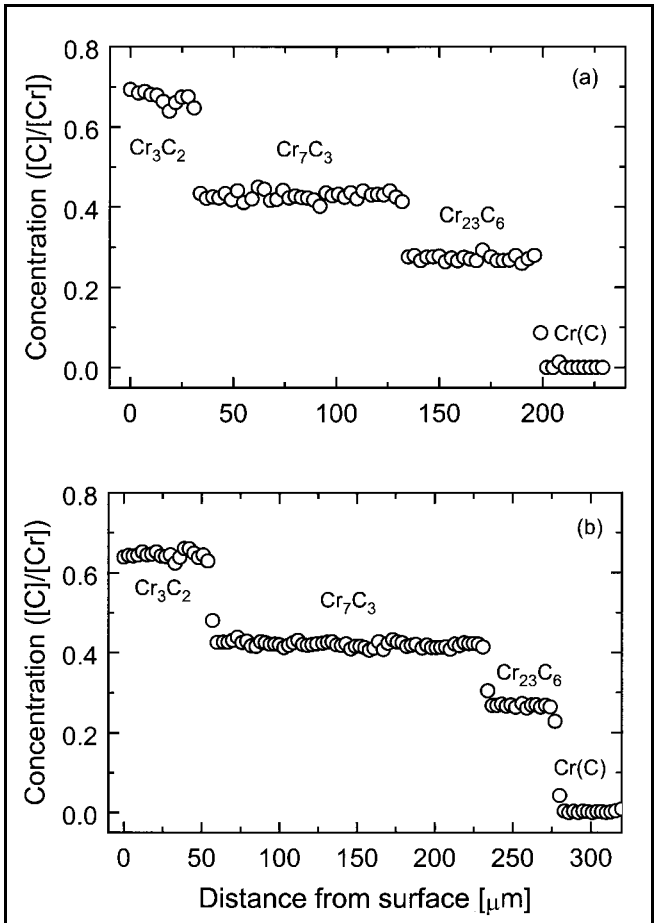

Fig. 4 Carbon profile across the chromium carbide diffusion couples. (a) Carbon profile across a wedge-type C/Cr diffusion couple (T = 1262 °C, t = 381 h). (b) Carbon profile across a plane-sheet Cr_3C_2/Cr diffusion couple (T = 1351 °C, t = 48 h)

is, 1369 °C, both microstructure features could be observed—the fine structure at the N-rich and the coarse structure at the N-poor side of δCrN_{1-x} (Fig. 3a). This result is attributed to the fact that during decomposition of δCrN_{1-x} the N atoms migrate only over shorter distances upon cooling from lower annealing temperatures, whereas at higher temperatures the migration distance is greater and hence coarser structures (lamellae) are formed. The fact that both coarse and fine structures were

Table 2 Homogeneity regions and lattice parameters of chromium carbides and chromium nitrides

Phase	Carbon/nitrogen concentration(a)				Lattice parameter, Å			Reference
	Lower limit, at.%	Upper limit, at.%	Lower limit mol/cm^3	Upper limit mol/cm^3	*a*	*b*	*c*	
$Cr_{23}C_6$	20.90(b)	21.37(b)	0.0088(b)	0.0091(b)	2.885	…	…	[62Mei]
Cr_7C_3	29.53(b)	29.71(b)	0.0217(b)	0.0219(b)	4.526	7.010	12.120	[70Rou]
Cr_3C_2	38.96(b)	39.35(b)	0.0472(b)	0.0478(b)	5.540	2.830	11.470	[62Mei]
β-Cr_2N	25.07(c)	32.91(c)	0.0396(c)	0.0543(c)	4.751	…	4.430	[67Sch]
δ-CrN_{1-x}	41.48(c)	47.48(c)	0.0674(c)	0.0810(c)	4.141	…	…	[71Nas]

(a) Lower limit means the C or N concentration at the C- or N-poor phase boundary; upper limit is the one at the C- or N-rich phase boundary in the phase diagram. (b) At 1262 °C. (c) At 1292 °C

Table 3 Diffusion coefficients of C in chromium carbides and in Cr calculated from the positions of phase boundaries observed in wedge-shaped diffusion couples

Temperature (*T*), °C	Diffusion coefficients, cm^2/s			
	Cr_3C_2	Cr_7C_3	$Cr_{23}C_6$	Cr(C)
1262	5.00×10^{-11}	2.00×10^{-10}	5.22×10^{-11}	7.60×10^{-10}
1323	1.50×10^{-10}	4.29×10^{-10}	1.15×10^{-10}	1.20×10^{-9}
1351	1.85×10^{-10}	6.72×10^{-10}	3.25×10^{-10}	2.00×10^{-9}
1369	1.32×10^{-10}	7.50×10^{-10}	1.32×10^{-10}	3.50×10^{-9}
1374	2.00×10^{-10}	9.65×10^{-10}	3.00×10^{-10}	2.50×10^{-9}
1412	1.95×10^{-10}	1.70×10^{-9}	4.60×10^{-10}	5.00×10^{-9}
1413	5.25×10^{-10}	1.15×10^{-9}	4.60×10^{-10}	4.50×10^{-9}

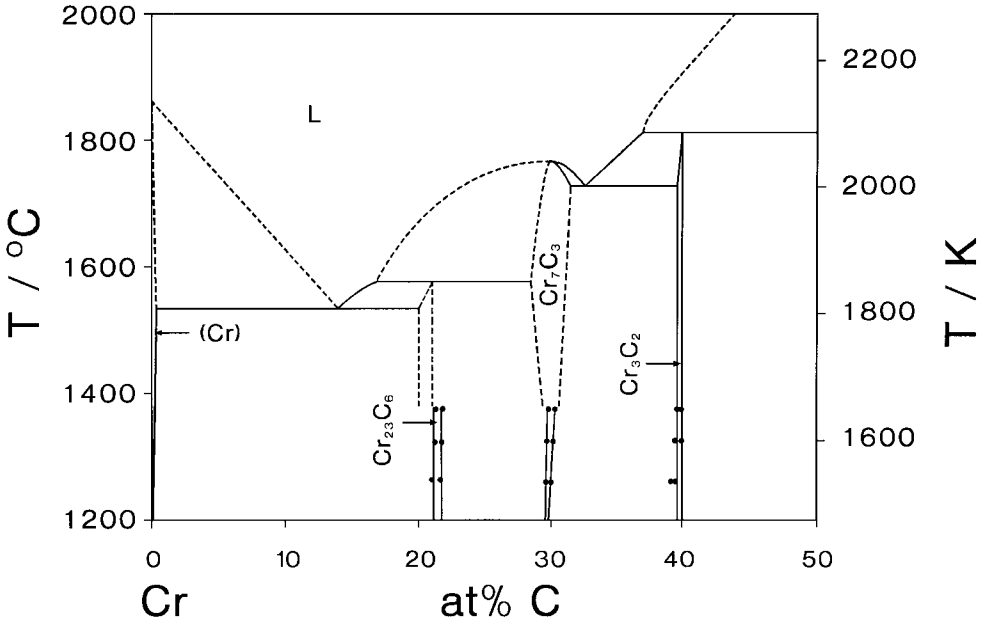

Fig. 5 Phase diagram of the Cr-C system [90Mas] with data for the homogeneity ranges of the chromium carbides obtained in the present study.

observed at an intermediate temperature range (1300 to 1400 °C) stems from the fact that the N-poor phase boundary of the δCrN_{1-x} significantly shifts toward the N-poor composition upon increasing temperature (see "Cr-N System" in section 3.2). Thus, the N-poor parts of the CrN_{1-x} phase band enter earlier, and thus at higher temperatures, than do the N-rich parts into the two-phase region upon cooling; the N atoms migrate over longer distances in the former as compared to the latter.

In order to avoid decomposition upon cooling from higher temperatures, the samples were dropped into liquid Sn (as described in section 2.1). This procedure could not prevent decomposition, but at least yielded a fine-grained microstructure.

3.2 Electron Probe Microanalysis

Cr-C System. High porosity in specimens made it difficult to perform line scans. Therefore Cr/C, $Cr_{23}C_6$/C, and Cr_7C_3/C diffusion couples being annealed at $T > 1413$ °C could not be investigated by EPMA. A typical line scan across a Cr/C diffusion couple and a Cr_3C_2/Cr diffusion couple, respectively, is presented in Fig. 4(a) and (b). The C profile shows only very small homogeneity ranges for all three phases. The data from EPMA were introduced into the Cr-C phase diagram presented in Fig. 5. A slightly higher C content in the $Cr_{23}C_6$ phase compared to the assessed phase diagram [90Mas] was found. The position of the other phases was in agreement with compiled data. The homogeneity ranges of the Cr-C phases were established to be very narrow (see Table 2).

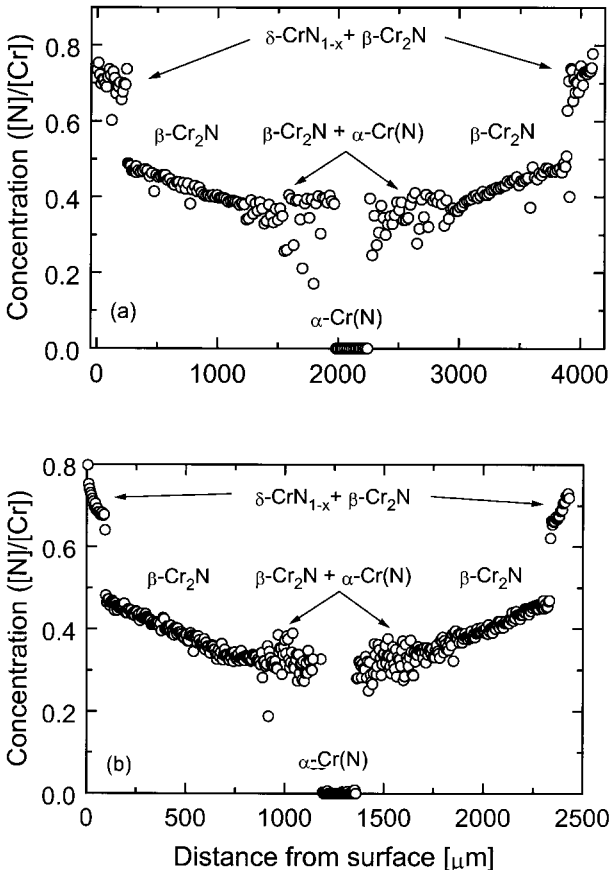

Fig. 6 Nitrogen profile across the chromium nitride diffusion couples. (a) Nitride profile in a wedge-type Cr/N diffusion couple (T = 1369 °C, p = 30.9 bar N_2, t = 24.4 h) with the coarse and fine microstructure (see Fig. 3a). (b) Nitrogen profile in a quenched wedge-type Cr/N diffusion couple (T = 1370 °C and p = 31.2 bar N_2, t = 10.0 h) with the fine microstructure only (see Fig. 3b)

Cr-N System. Several chromium nitride diffusion couples were investigated by means of EPMA. A line scan across a Cr-N diffusion couple annealed at 1369 °C (Fig. 6a) shows a scattered nitrogen profile for the δ-CrN_{1-x} phase bands and the nitrogen-poor region of the β-Cr_2N phase bands due to decomposition upon cooling (compare with Fig. 3a for the δ-CrN_{1-x} phase band). Upon quenching the samples into liquid Sn the decomposition could not be avoided but only a fine-grained structure occurred leading to a smooth nitrogen profile in the δ-CrN_{1-x} phase upon EPMA (Fig. 6b). This broadening was also observed in samples cooled from 1231 and 1292 °C or quenched from 1420 °C; all of which showed a fine-grained microstructure such as given in Fig. 3(b). At T = 1155 °C the homogeneity range was found to be very small.

The data observed from EPMA were introduced into the Cr-N phase diagram in Fig. 7 [90Mas]. In contrast to the assessed phase diagram the δCrN_{1-x} phase was found to be no line compound at higher temperature. The N-poor boundary of δCrN_{1-x} shifts substantially toward lower N content with increasing temperature. The N-rich boundary depends, of course, on the N_2 pressure. In order to obtain a composition of 50 at.%, substantially higher N_2 pressures would be required than accessible in the present study (maximum 31 bar N_2).

3.3 Diffusion Coefficients

The diffusion coefficients of C and N in Cr, chromium carbides, and chromium nitrides, respectively, were obtained by investigating the layer growth in wedge-shaped diffusion couples. The authors assumed that the diffusivity of the metal is negligible in comparison with the diffusivity of the nonmetal in the Cr-C and Cr-N systems.

The deviations from the parabolic layer growth observed in wedge-shaped diffusion couples allowed the diffusion coefficients in all phases to be calculated from the interphase boundaries [97Raf1]. For the calculation of diffusion coefficients, a forward finite difference (FFD) method was applied [97Raf2]. Using this technique, the positions of phase boundaries were calculated for a given diffusion time and fitted on the observed sample microstructure by refining the diffusion coefficients in individual phases. The maximum and the minimum concentrations within the respective phase were taken from the EPMA measurements (Table 2).

Cr-C System. The diffusion coefficients calculated for Cr(C) and for the chromium carbide phases $Cr_{23}C_6$, Cr_7C_3, and Cr_3C_2 in the range 1262 to 1413 °C are summarized in Table 3 and shown in form of the Arrhenius dependence in Fig. 8. The activation energies and the pre-exponential factors of the diffusion coefficients are given in Table 4. With respect to the extremely narrow homogeneity ranges in all phases, the diffusion coefficients in the Cr-C system were assumed to be independent of the C concentration. The data are somewhat scattered because homo-

geneity ranges of phases with an almost line-compound character are measured with great difficulty and the relative error is much greater than in phases with a broad homogeneity range. Thus it will be proved in further studies whether the calculation of integrated diffusion coefficients [98Loo] is more appropriate and compares with the results of this study.

Cr-N System. For δCrN_{1-x} and βCr_2N having rather broad homogeneity ranges, the concentration-independent diffusion coefficients obtained from layer growth (as for the Cr-C system) were compared with the concentration-dependent diffusion coefficients calculated from the shape of the concentration profiles measured using EPMA (see section

Table 4 Activation energies and the preexponential factors in the Cr-C system

Phase	Cr_3C_2	Cr_7C_3	$Cr_{23}C_6$	Cr(C)
Activation energy (E), eV	2.5 ± 0.6	2.9 ± 0.2	3.2 ± 0.6	2.9 ± 0.3
Preexponential factors (D_0, cm^2/s	1.21×10^{-2}	0.718	1.28	1.54

Table 5 Diffusion coefficients of N in the Cr-N system as calculated from the positions of phase boundaries (FFD) and from the shape of the measured concentration profiles

Temperature	FFD, cm^2/s			Analysis of the concentration profiles, cm^2/s		
(T), °C	δCrN_{1-x}	βCr_2N	$\alpha Cr(N)$	$\delta CrN_{1.00}$	$\delta CrN_{0.67}$	βCr_2N
1155	2.20×10^{-11}	1.30×10^{-9}	4.00×10^{-9}	1.00×10^{-12}	2.75×10^{-10}	1.01×10^{-9}
1231	1.57×10^{-10}	3.59×10^{-9}	1.00×10^{-8}	2.96×10^{-12}	8.90×10^{-10}	3.20×10^{-9}
1292	8.83×10^{-10}	6.50×10^{-9}	2.00×10^{-8}	7.00×10^{-12}	2.35×10^{-9}	6.34×10^{-9}
1369	5.10×10^{-9}	2.17×10^{-8}	6.50×10^{-8}	2.00×10^{-11}	6.52×10^{-9}	
1370	5.17×10^{-9}	1.78×10^{-8}	6.50×10^{-8}	2.05×10^{-11}	6.60×10^{-9}	2.62×10^{-8}
1420	1.37×10^{-8}	4.35×10^{-8}	1.45×10^{-7}			

The concentration profiles were extrapolated for $\delta CrN_{1.00}$ and $\delta CrN_{0.67}$, which allowed the temperature dependence and the concentration dependence of the diffusion coefficient to be separated.

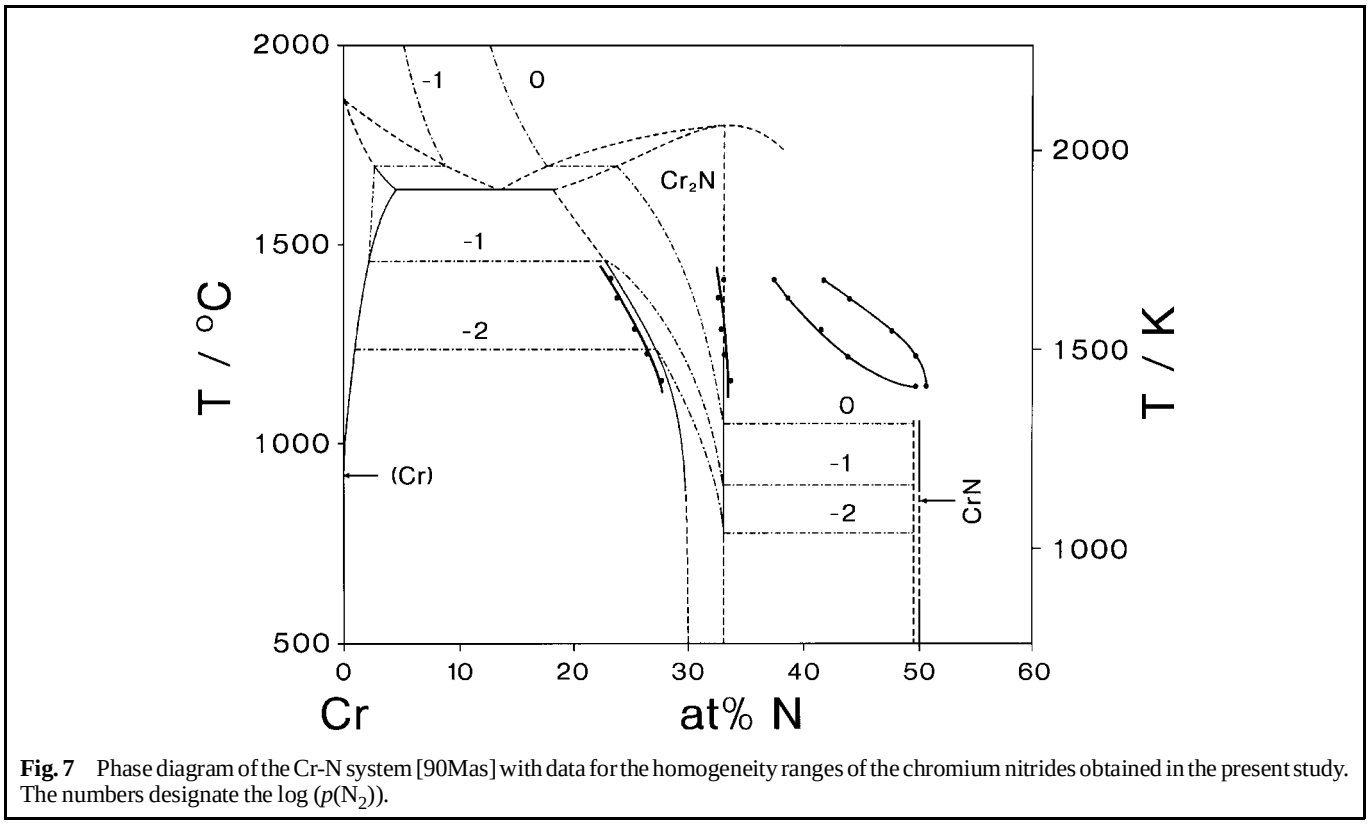

Fig. 7 Phase diagram of the Cr-N system [90Mas] with data for the homogeneity ranges of the chromium nitrides obtained in the present study. The numbers designate the log ($p(N_2)$).

3.2). The experimental concentration profiles were approximated by the function [97Raf1]:

$$c(y) = (c^- - c^+)\left[\int_{y(0)}^{y} \frac{1}{D(y')} \exp\left(-\int_{y(0)}^{y} \frac{2y''\,dy''}{D(y'')}\right)dy'\right] \div \left[\int_{y(0)}^{y(\xi)} \frac{1}{D(y')} \exp\left(-\int_{y(0)}^{y} \frac{2y''\,dy''}{D(y'')}\right)dy'\right] + c^+ \qquad \text{(Eq 1)}$$

in which the concentration dependence of the diffusion coefficient D was described by the well-established exponential function [89Loo]:

$$D(c) = D_0 \exp\,[a(c^+ - c)] \qquad \text{(Eq 2)}$$

In Eq 1, $y(0)$ and $y(\xi)$ denote the beginning and the end of the respective concentration profile written in terms of the Boltzmann-Matano variable, $y = x/(2\sqrt{t})$; c^+ and c^- are the maximum and the minimum N concentrations in mol N/cm^3. The free parameters of the diffusion coefficients, D_0 and a, were refined within the calculation (Eq 2).

The diffusion coefficients obtained in all phases (δCrN_{1-x}, βCr_2N, and $\alpha Cr(N)$) are summarized in Table 5, which also gives the comparison between the concentration-independent and the concentration-dependent diffusion coefficients. The temperature dependence of the diffusion coefficients is shown in Fig. 9. The activation energies and the preexponential factors calculated from the respective set of the diffusion coefficients are listed in Table 6. The comparison of the activation energy and preexponential factor with the literature data was only possible for βCr_2N as the diffusion coefficients in other phases have not been reported yet. The diffusion coefficients given by [81Mil] yielded the activation energy of 2.34 ± 0.03 eV and the preexponential factor of 5.4 ± 1.5 cm^2/s, which is in accordance with the authors' results.

A significant concentration dependence of the diffusion coefficient was found for the δCrN_{1-x} phase. The analysis of the measured concentration profiles yielded that the N diffusivity in δCrN_{1-x} decreases with increasing N concentration. This can already be seen from the shape of the concentration profiles near the sample surface (Fig. 10), where a very high compositional gradient was found. The solid line, which represents the concentration profile calculated with the

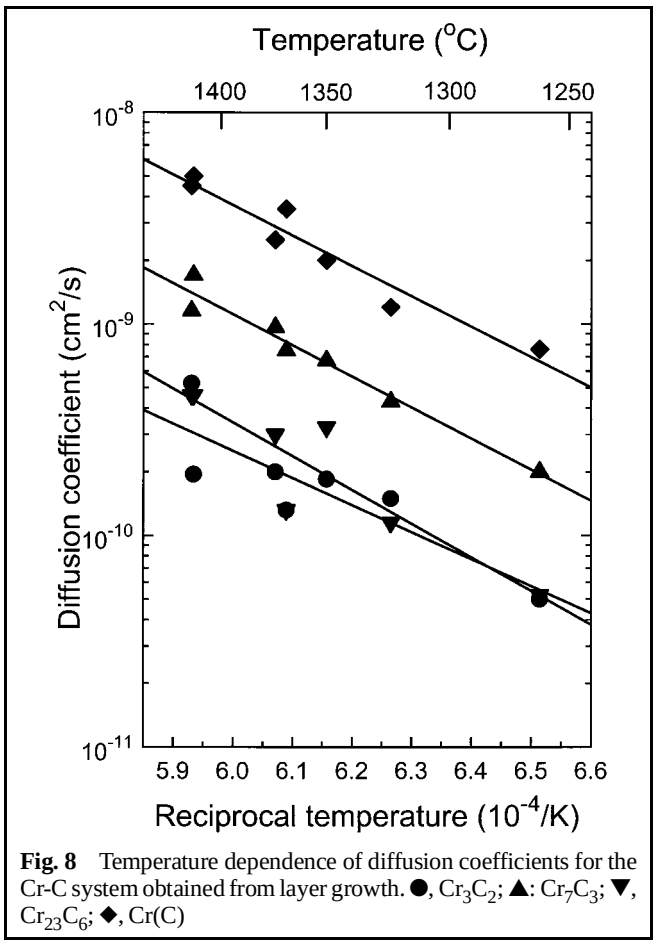

Fig. 8 Temperature dependence of diffusion coefficients for the Cr-C system obtained from layer growth. ●, Cr_3C_2; ▲: Cr_7C_3; ▼, $Cr_{23}C_6$; ◆, Cr(C)

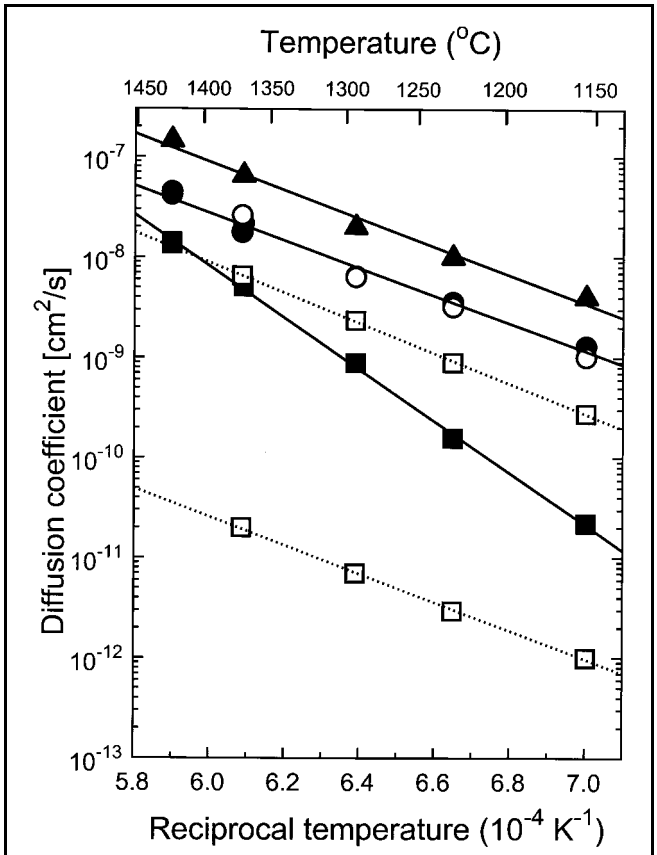

Fig. 9 Temperature dependence of diffusion coefficients for the Cr-N system as obtained from layer growth (solid symbols, solid lines) and from the concentration profile fitting (open symbols, dashed lines). ♦ /■, δCrN_{1-x}; ϒ /●, βCr_2N; ▲, $\alpha Cr(N)$. The diffusion coefficients of N in δCrN_{1-x} calculated from layer growth correspond to different N concentrations at different temperatures, and therefore the Arrhenius dependence yields a higher activation energy (see text). The diffusion coefficients obtained using the concentration profile fitting correspond to $CrN_{1.00}$ (lower dashed line) and $CrN_{0.67}$ (upper dashed line). The latter is not stable at lower temperatures (see Fig. 7).

concentration-dependent diffusion coefficients approximates well the measured concentrations (open circles), whereas larger differences can be seen in the second fit, in which the concentration dependence of the diffusion coefficient was omitted (dashed line).

The dependence of the N diffusion coefficient on the temperature and N concentration in δCrN_{1-x} could be described by the exponential surface:

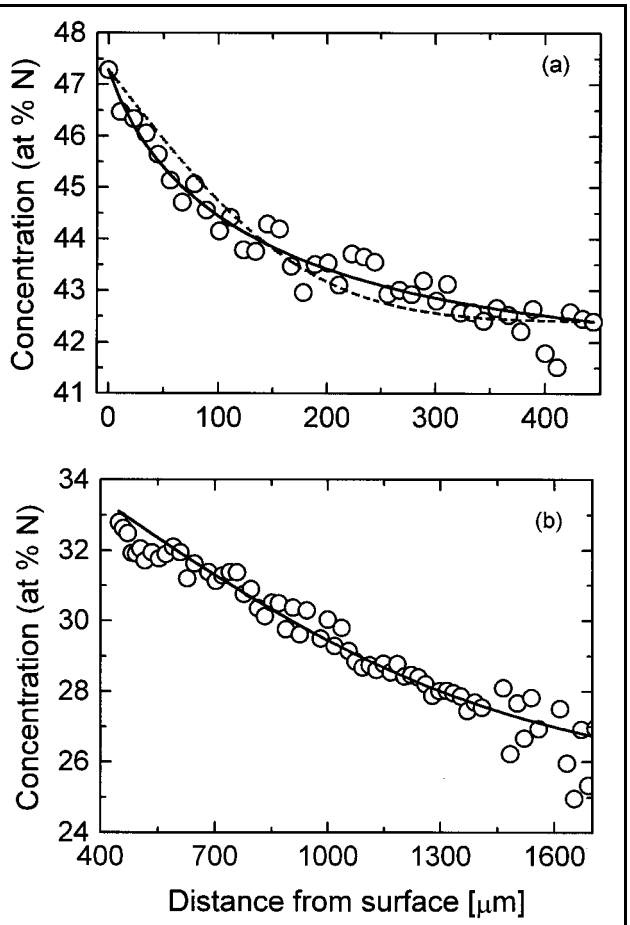

Fig. 10 (a) Comparison of the theoretical concentration profiles in δCrN_{1-x} calculated with the concentration-independent (dotted line) and the concentration-dependent diffusion coefficients (solid line) of N. The measured concentration profile is plotted by open circles. (b) Concentration profile calculated with the concentration-independent diffusion coefficient. The line approximates the measured concentration profile well, which means that no significant concentration dependence of the N diffusion coefficient exists for βCr_2N.

$$D\,[\mathrm{cm^2/s}] = 0.018 \times \exp\left(-\frac{2.92\ \mathrm{eV}}{k_B T}\right) \times \exp\,(17.2x) \qquad \text{(Eq 3)}$$

where k_B is the Boltzmann constant, T the temperature, and x is the atomic fraction of N in δCrN_{1-x}. The activation energies calculated for isoconcentration cuts (dashed lines in Fig. 9) are identical for all concentrations within the experimental precision and lower than the activation energy obtained from the concentration-independent diffusion coefficients. Note that data for 40 and 50 at.% N (open boxes in Fig. 9) illustrate the concentration dependence of the diffusion coefficient, which is approximately two orders of magnitude. The N concentration of 40 at.% N, however, does not occur at some (lower) temperatures as it follows from the phase diagram. Also, the N concentration of 50 at.% N has not been reached at all temperatures because much larger N pressures than accessible in this study would have to be applied.

The strong concentration dependence of the diffusion coefficient in δCrN_{1-x} can also explain why too high an activation energy was obtained from the concentration-independent diffusion coefficients (Table 6). The reason is that the FFD calculation yielded diffusion coefficients for different mean nonmetal concentrations at different temperatures because the homogeneity range of δCrN_{1-x} shifts to lower concentrations with increasing temperature (Fig. 7). Thus, the calculation of activation energy at nonequal concentrations resulted in an oblique cut on the exponential surface, which consequently yielded a much higher activation energy for δCrN_{1-x} (broken line in Fig. 11).

On the contrary, no remarkable concentration dependence of the diffusion coefficients was observed in βCr_2N. The measured concentration profiles in βCr_2N could be well approximated by concentration profiles calculated using Eq 1 with concentration-independent diffusion coefficients (see Fig. 10). The diffusion coefficients calculated from the positions of phase boundaries and from the concentration profiles in βCr_2N agree well (Fig. 9).

3.4 Microhardness

The microhardness of the chromium carbide phases increases with increasing C content (Fig. 12a). Two series of measurements on either side of the Cr_7C_3 phase band indicate an increase of Vickers hardness with increasing C content, too. Literature data [53Hin] as well as the authors' microhardness values are given in Table 7.

The microhardness measurements on chromium nitride diffusion layers yielded a general increase of the Vickers microhardness with increasing N content. Within the phase, a substantial increase was found for βCr_2N and a decrease for

Table 6 Activation energies and preexponential factor evaluated from the temperature dependence of the concentration-independent (FFD) and the concentration-dependent diffusion coefficient (calculated from the concentration profiles) in the Cr-N system

	FFD			Concentration profiles	
	δCrN_{1-x}	βCr_2N	$\alpha Cr(N)$	$\delta CrN_{1.00}$	$\delta CrN_{0.67}$
Activation energies (E), eV	5.12 ± 0.08	2.68 ± 0.15	2.79 ± 0.15	2.83 ± 0.10	3.01 ± 0.10
Preexponential factor (D_0, cm^2/s	2.43×10^7	3.51	23.9	9.21×10^{-3}	11.0

δCrN_{1-x} (Fig. 12b, Table 7). It is clear that the two-phase structure of δCrN_{1-x} could affect the hardness. However, such a behavior was also found for isostructural nitrides of the V-N, Nb-N, and Ti-N systems [85Len, 86Len, 92Len]. This behavior might be attributed to the increasing occupancy of antibonding states with increasing N content at valence electron concentrations greater than 8.

4. Conclusions

The layer growth in the Cr-C and Cr-N systems was investigated by the means of reaction diffusion couples. The carbides were prepared by reaction of compact Cr metal with graphite powder under argon atmosphere. Nitride samples were prepared by reaction of pure Cr metal with N up to 31 bar. While the carbide samples showed three chromium carbide phases in form of dense diffusion layers between 1143 and 1413 °C; at $T \geq$ 1413 °C, high porosity occurred. At sample thickness that allows the diffusion geometry to be regarded as infinite, the Cr_7C_3 phase is about twice as thick as the other two phases. The composition of the phase bands was measured by EPMA; the results were adopted for a modification of the Cr-C phase diagram. The following C diffusivities were obtained from layer-thickness measurements in wedge-shaped diffu-

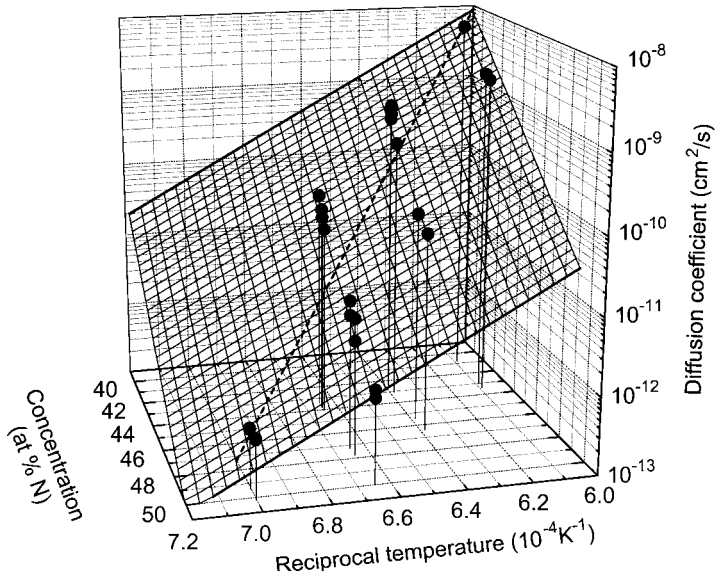

Fig. 11 Exponential surface describing both the temperature and concentration dependence of the N diffusion coefficient in δCrN_{1-x}. Balls are the measured diffusion coefficients; the surface is characterized by Eq 3. Solid lines at 40 and 50 at.% N represent the true Arrhenius dependence of the diffusion coefficient. The dashed line is obtained if the mean concentrations are used for calculating the diffusion coefficient.

Table 7 Vickers microhardness with standard deviation of several chromium carbide and nitride phases obtained on sample 053ECrC and 054ECrN together with some literature values

Phase	Nonmetal content, at.% C or at.% N	Vickers hardness, GPa	Standard deviation (σ), GPa	Vickers hardness from literature(a), GPa
Cr_3C_2	39.2	26.6	1.5	26.5 [53Hin]; 13.8 [64Sam]
Cr_7C_3	29.7	23.6	2.5	20.6 [53Hin]; 13.6 [64Sam]
	29.5	20.2	1.6	…
$Cr_{23}C_6$	21.1	14.1	1.4	16.2 [53Hin]; 16.8 [64Sam]
αCr(C)	0.0(b)	9.6	0.2	…
δCrN_{1-x}	45.6	12.8	1.0	11.1 [64Sam] (49.7at.% N)
	43.5	14.0	0.8	…
βCr_2N	32.9	12.5	0.4	16.0 [64Sam] (32.3 at.% N)
	31.6	12.0	0.3	…
	30.0	11.6	0.6	…
	28.4	10.2	0.3	…
	27.5	10.0	0.8	…
αCr(N)	0.5(c)	7.2	0.5	…

(a) These values were measured at a load of 4.81 N on the polished surface of the samples. (b) The C content of αCr(C) at 1260 °C is about 0.03 at.% C [85Pou]. (c) The N content of a Cr(N) at 1231 °C is about 0.51 at.% N [71Mil].

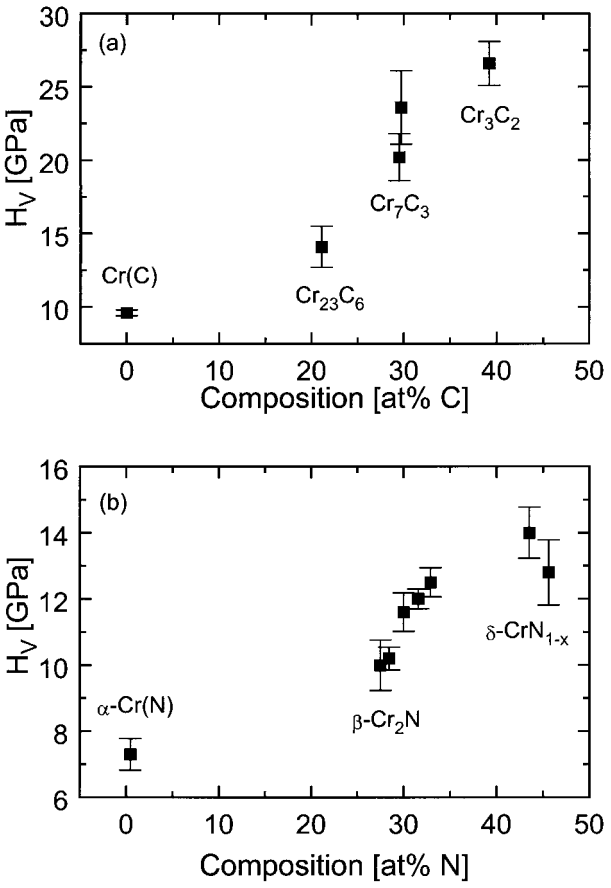

Fig. 12 Microhardness of several chromium carbide and nitride phases as a function of the nonmetal concentration (correlated with EPMA scans). The error bars indicate the standard deviations. (a) Cr-C system, the values were obtained on a sample annealed at 1262 °C. (b) Cr-N system, the values were obtained on a sample annealed at 1292 °C

sion couples: $D_C = 1.54 \times \exp(-2.9\ eV/k_BT)$ in Cr; $D_C = 1.28 \times \exp(-3.2\ eV/k_BT)$ in $Cr_{23}C_6$; $D_C = 0.72 \times \exp(-2.9\ eV/k_BT)$ in Cr_7C_3, and $D_C = 1.21 \times 10^{-2} \times \exp(-2.5\ eV/k_BT)$ in Cr_3C_2.

In the Cr-N system, both the δCrN_{1-x} and βCr_2N formed phase bands at $T \geq 1155$ °C. Both nitrides decomposed upon cooling especially in the N-poor region of the layers. Therefore, different microstructures were observed depending on the annealing temperature. Quenching experiments were carried out in the range 1370 to 1420 °C at 31 bar N_2 to stabilize the phases. The EPMA investigations of the homogeneity ranges in both phases yielded that the homogeneity range of δCrN_{1-x} is substantially higher than at lower temperatures. The following diffusion coefficients of N in the Cr-N system were calculated from the layer growth: $D_N = 0.018 \times \exp(-2.92\ eV/k_BT) \times \exp(17.2x)$ in δCrN_{1-x}, $D_N = 3.51 \times \exp(-2.68\ eV/k_BT)$ in βCr_2N, and $D_N = 23.9 \times \exp(-2.79\ eV/k_BT)$ in αCr. The microhardnesses generally increase with increasing nonmetal content, except for δCrN_{1-x}.

Acknowledgment

This project was supported by the Austrian National Science Foundation (FWF) under the Project No. P11178-PHY and M-00315-CHE, and by the Austrian Academy of Science under the Project No. PICS-134. The authors would like to thank Mr. M. Ostermann, Teledyne Metalworking Products, Huntsville, AL (USA) for supplying Mo sheets.

References

53Hin: J. Hinnüber and O. Rüdiger, *Arch. Eisenhüttenwes.*, Vol 24, 1953, p 267

62Mei: D. Meinhardt and O. Krisement, *Arch. Eisenhüttenwes.*, Vol 33, 1962, p 493

64Sam: G.V.Samsonov, *Handbook of High-Temperature Materials*, No. 2, Plenum Press, 1964

67Sch: K. Schwerdtfeger, *Trans. AIME*, Vol 239, 1967, p 1432

68Fri: R.J. Fries, J.E. Cummings, C.G. Hoffmann, and A. Daily, *6. Plansee Seminar*, Vol XXIX, 1968, p 568

70Rou: A. Rouault, P. Herpin, and R. Fruchart, *Ann. Chim.*, Vol 5 (No. 6), 1970, p 461

71Mil: T. Mills, *J. Less-Common Met.*, Vol 23, 1971, p 317

71Nas: M. Nasr-Eddine and E.F. Bertaut, *Solid State Commun.*, Vol 9, 1971, p 717

81Mil: T. Mills, *Oxid. Met.*, Vol 15, 1981, p 437

85Len: W. Lengauer and P. Ettmayer, *J. Less-Common Met.*, Vol 109, 1985, p 351

85Pou: J.J. Poubeau and J. Bigot, *Acta Metall.*, Vol 33 (No. 6), 1985, p 1137

86Len: W. Lengauer and P. Ettmayer, *Monatsh. Chem.*, Vol 117, 1986, p 275

89Loo: F.J.J. van Loo and G.F. Bastin, *Metall. Trans. A*, Vol 20, 1989, p 403

90Mas: T.B. Massalski, Ed., *Binary Alloy Phase Diagrams*, ASM International, 1990

90Ven: M. Venkatraman and J.P. Neumann, *Bull. Alloy Phase Diagrams*, Vol 11, 1990, p 152

92Len: W. Lengauer, *J. Alloys Compd.*, Vol 186, 1992, p 293

93Len: W. Lengauer, D. Rafaja, R. Täubler, C. Kral, and P. Ettmayer, *Acta Metall. Mater.*, Vol 41 (No. 12), 1993, p 3505

95Len: W. Lengauer, *J. Alloys Compd.*, Vol 229, 1995, p 80

96Neu: J. P. Neumann, University of Wisconsin, private communication, 1996

96Raf: D. Rafaja, W. Lengauer, and P. Ettmayer, *Acta Mater.*, Vol 44 (No. 12), 1996, p 4835

97Len: W. Lengauer, J. Bauer, M. Bohn, H. Wiesenberger, and P. Ettmayer, *Mikrochim. Acta*, Vol 126, 1997, p 279

97Raf1: D. Rafaja, W. Lengauer, H. Wiesenberger, and M. Joguet, *Metall. Mater. Trans. A*, Vol 29A, 1998, p 439-446

97Raf2: D. Rafaja and W. Lengauer, *Modelling and Simul. Mater. Sci. Eng.*, Vol 6, 1998, p 141-152

98Wie: H. Wiesenberger, W. Lengauer, and P. Ettmayer, *Acta Mater.*, Vol 46 (No. 2), 1998, p 651

98Loo: F.J.J. van Loo, private communication, 1998